applied sciences

Article

Assessing the Suitability of Damage Indexes for Digital Twin Applications in RC Buildings Considering Masonry Infills

Luca Danesi, Andrea Belleri *, Michelle Gualdi and Simone Labò

Department of Engineering and Applied Sciences, University of Bergamo, Viale Marconi 5, 24044 Dalmine, Italy; luca.danesi@unibg.it (L.D.); michelle.gualdi@unibg.it (M.G.); simone.labo@unibg.it (S.L.)
* Correspondence: andrea.belleri@unibg.it

Abstract: Given the significant damage caused by earthquakes over the years, accurate prediction and assessment of the extent of structural damage is critical to ensure safety and guide post-disaster recovery efforts. This study examines the effectiveness and reliability of various damage indexes for reinforced concrete buildings, particularly in the context of seismic events. It highlights the potential of these indexes for future use in digital twin applications or for direct analysis of sensor data recorded during an earthquake, with the ultimate goal of improving real-time damage assessment and decision making. A comprehensive literature review was carried out looking at the damage indexes developed over the last decades. These indexes were applied to a case study involving an RC building with three different structural configurations: a pre-code moment-resisting frame, a code-compliant moment-resisting frame, and a code-compliant shear wall system, both bare and infilled with masonry. The seismic performance of these configurations was evaluated using Multi-Stripe Analyses (MSA) to account for the variability of the seismic input. The results of applying the damage indexes highlight the versatility of these indexes in detecting damage, although some limitations were noted, particularly with cycle-related indicators and their application to infilled structures. The study emphasizes the importance of refining these tools to improve their accuracy and reliability in different structural contexts, ultimately contributing to more accurate seismic damage assessment and damage prediction for specific seismic scenarios.

Keywords: damage index; masonry infills; RC buildings; seismic damage

check for updates

Academic Editor: Maria Favvata

Received: 17 January 2025
Revised: 6 February 2025
Accepted: 11 February 2025
Published: 14 February 2025

Citation: Danesi, L.; Belleri, A.; Gualdi, M.; Labò, S. Assessing the Suitability of Damage Indexes for Digital Twin Applications in RC Buildings Considering Masonry Infills. *Appl. Sci.* **2025**, *15*, 1999. https://doi.org/10.3390/app15041999

1. Introduction

Earthquakes pose a significant threat to human life, infrastructure and the economy worldwide. Past earthquakes have shown how vulnerable the existing building stock is to both direct and indirect losses, with the latter being more difficult to quantify and often overlooked in damage assessments. For example, the economic losses caused by the disruption of services or the interruption of industrial production are particularly difficult to estimate.

Nowadays, there is a growing interest in quantifying and assessing potential building damage using specialized methods. Accurate prediction of expected damage prior to an earthquake based on factors such as building design, building materials, seismic retrofitting and historical earthquake data is crucial for urban planning, risk mitigation strategies and insurance. Similarly, effective damage assessment that evaluates the actual damage after the earthquake plays an important role in guiding emergency response, repair efforts and reconstruction, as well as refining future predictive models.

In recent decades, numerous formulations for the calculation of damage indexes have emerged that provide clear and standardized definitions for expected and actual damage. These methods cover both the prediction of damage before an event and the assessment of damage after an event. In this study, the damage indexes developed in recent decades to assess the seismic damage condition of buildings are examined in a comprehensive literature review. The indexes assessment is performed through Multi-Stripe Analyses (MSA), which take into account the variability of the seismic input for a more robust understanding of the potential damage scenarios. Specifically, the study considers six selected damage indexes and a reinforced concrete (RC) reference building with different structural configurations: a pre-code frame system, a code-compliant moment-resisting frame system and a code-compliant shear wall system. Both the bare frame and the masonry-infilled configurations are analyzed.

In this context, the potential application of damage indexes in digital twins and sensor-based systems is emphasized. Through a non-linear dynamic analysis performed on digital twins, damage indexes can be calculated in near real time, allowing for a fast and accurate post-event assessment. This approach provides a robust tool for continuous structural health monitoring and facilitates the simulation of different earthquake scenarios to better understand and prepare for potential risks. Similarly, the use of the data recorded by the sensors and their elaboration, such as floor accelerations and inter-storey displacements, may enable the calculation of damage indexes without requiring a finite element model. This enables rapid quantification of damage to buildings, including structural and non-structural components, and provides information for timely decision making for emergency response and repair strategies.

In this study, we provide a comprehensive overview of selected damage indexes for the assessment of seismic damage to buildings, validate their effectiveness and highlight their strengths and limitations. The main novelty of this work lies in the comprehensive evaluation of the effectiveness and reliability of damage indexes thorough Multi-Stripe Analyses (MSA) and in the proposal of specific formulations for the consideration of masonry infills. The use of MSA is particularly important to understand how each index performs in different structural configurations—such as existing buildings, code-compliant framing systems and code-compliant wall systems—and how accurately they quantify damage at different limit states.

The effectiveness of the damage indexes in the analyses carried out on finite element models suggests that these indicators can also be widely applied to digital twin models. Damage indexes can be implemented in digital twin models to assess potential damage due to extreme events such as earthquakes in near real time. The knowledge gained from this study will help to select the most appropriate existing index to assess the predicted and expected damage in different scenarios, considering both serviceability and collapse conditions. The same procedure could also be used to evaluate the effectiveness of new damage indexes.

2. Seismic Damage Indexes for RC Buildings

The growing interest of the scientific community in damage detection and control in buildings has led to the definition of a variety of damage indexes that can express the condition of structural elements and components or the entire building after a seismic event by a scalar measure [1]. Since the 1970s, systematic attempts have been made to quantitatively estimate the local or global extent of seismic damage to structural systems. In the past, the damage indexes for reinforced concrete (RC) buildings proposed in the literature have been extensively discussed and studied [2,3]. This section presents the main damage indexes that have been developed to assess local damage to RC structural members, as well as a global index suitable for assessing the overall damage of the whole building.

As for the local damage in a single element, Lybas and Sozen (1977) [4] introduced the following index:

$$DI_{\mathrm{L-S}} = \frac{k_0}{k_m} \quad (1)$$

where k_0 and k_m are the elastic and the secant stiffness at the maximum displacement, respectively.

Assuming a monotonically increasing load path, this index starts at a value of 1.0 in the undamaged state and gradually increases until it reaches a maximum value of 3.5 in the final state.

In the same year, a flexural damage index was introduced by Banon et al. (1977) [5]:

$$DI_{\mathrm{FDR}} = \frac{\frac{\phi_m}{M_m} - \frac{\phi_y}{M_y}}{\frac{\phi_u}{M_u} - \frac{\phi_y}{M_y}} \quad (2)$$

where ϕ_m, ϕ_y and ϕ_u are the maximum, yield and ultimate curvature, respectively, and M_m, M_y and M_u are the maximum, yield and ultimate bending moment, respectively. The index is designed to provide a value of zero in the absence of damage and to gradually increase to a value of 1.0 when the structure reaches its final state.

Banon and Veneziano (1982) [6] introduced the first damage index based on the dissipated energy, which is particularly relevant for cyclic loads, such as those experienced during seismic events. This index is calculated for each loading cycle:

$$DI_{\mathrm{B-V}} = \sqrt{\left(\frac{d_m}{d_y - 1}\right)^2 + \left[\left(\frac{2E_h}{F_y d_y}\right)^{0.38}\right]^2} \quad (3)$$

where d_m and d_y are the maximum and the yield displacement, respetively, F_y is the yield force and E_h is the dissipated energy. This damage index is calculated for each cycle and is defined as the maximum value among the indexes determined. It assumes values greater than zero even before the yield point and exceeds 9.0 under failure conditions.

Hwang and Scribner (1984) [7] defined the following index based on the dissipated energy:

$$DI_{\mathrm{H-W}} = \sum_{i=1}^{n} \frac{k_i {d_i}^2}{k_e {d_y}^2} \quad (4)$$

where k_e and k_i are the element's initial elastic flexural stiffness and the element's flexural stiffness at the i-th cycle, respectively, d_y and d_i are the element's yield displacement and the element's displacement at the i-th cycle, respectively, and n is the number of cycles. As can be seen from its mathematical formulation, the index represents the cumulative damage across all cycles. This results in values that are already greater than zero before the yield point and exceed 4.0 in the final state of the structural element.

The index proposed by Park and Ang (1985) [8] is

$$DI_{\mathrm{P-A}} = \frac{d_m}{d_u} + \frac{\beta}{F_y d_u}\int dE \quad (5)$$

in which

$$\beta = \left(-0.447 + 0.073\frac{L}{d} + 0.24n + 0.314\rho_t\right) \cdot 0.7^{\rho_\omega} \quad (6)$$

where d_u is the ultimate displacement under monotonic loading, d_m is the maximum displacement experienced during the earthquake, dE is the differential dissipated energy, L is the structural element length, d is the effective depth of the cross-section, n is the normalized axial load, ρ_t is the percentage of longitudinal reinforcement and ρ_{ϖ} is the confinement ratio. This index assumes values greater than zero when the element is undamaged and approaches a value of 2.0 when the element reaches failure.

Stephensen and Yao (1987) [9] introduced an index based on the cumulative displacement ductility:

$$DI_{\text{S}-\text{Y}} = \sum_{i=1}^{n} \left(\frac{\Delta d^{+}}{\Delta d_f} \right)^{1-b\cdot r} \quad (7)$$

where Δd^{+} and Δd^{-} are the incremental increase in the displacements of the element in the positive and negative direction, respectively, Δd_f is the collapse displacement, b is a coefficient that assumes a value of 0.77 and $r = \frac{\Delta d^{+}}{\Delta d^{-}}$ is the ratio between the two incremental increases. The sum of the damage over all cycles leads to a value greater than zero before the yielding point and greater than 1.0 when the structural element is approaching failure.

Wang and Shah (1987) proposed an index based solely on the forces and bending moment value experienced by the element [10]. However, this characteristic makes the index difficult to apply for real-time structural monitoring, as it requires specialized measurement equipment. The index can be computed as

$$DI_{\text{W}-\text{S}-1} = 1 - \frac{F_y}{F_m} \quad (8)$$

where F_y and F_m are, the yield and the maximum shear force or bending moment in the element during the cyclic loading, respectively.

This index assumes negative values under loading conditions below the yielding point, reaches 0.0 at the yielding point and generally approaches values close to 0.1 when the element reaches its maximum force during cyclic loading.

A second formulation of the index assumes that the damage to an RC member subjected to cyclic loading depends on the maximum displacements experienced by the element during each cycle [10]. A cyclic-loading parameter is defined as

$$\beta = C \cdot \sum_{i=1}^{n} \frac{\vartheta_i}{\vartheta_u} \quad (9)$$

where ϑ_i and ϑ_u are the rotation at the i-th cycle and the ultimate rotation of the section of the analyzed element, respectively. The index is computed as follows:

$$DI_{\text{W}-\text{S}-2} = \frac{e^{\eta\beta} - 1}{e^{\eta} - 1} \quad (10)$$

where η can be -3 and -1 while C is a constant equal to 0.15.

This index assumes values greater than zero even before the element reaches the yield point and remains below 0.2 as the structural element approaches failure.

Powell and Allahabadi (1988) [11] developed an index for RC elements based on plastic deformation and displacement ductility:

$$DI_{\text{P}-\text{Al}} = \frac{\mu_m - 1}{\mu_u - 1} \quad (11)$$

where μ_m is the maximum ductility experienced by the element and μ_u is the ultimate ductility of the element. The mathematical formulation of the index defines values between 0.0 and 1.0, corresponding to no-damage and failure conditions, respectively.

As for the global damage of a structure, Di Pasquale and Cakmak (1988) [12] presented an index based on the variation of the fundamental period of vibration of the structure following an earthquake:

$$DI_{\text{DP-C}} = 1 - \frac{T_a}{T_m} \tag{12}$$

where T_a and T_d are the initial and final fundamental period of vibration of the structure, respectively.

Bracci et al. (1989) [13] suggested a damage index based on the residual curvature of the structural element:

$$DI_{\text{Br-al}} = \frac{\varphi_m - \frac{M_u}{k_m}}{\varphi_u - \frac{M_u}{k_u}} \tag{13}$$

where φ_m and φ_u are the maximum and ultimate curvature, respectively, M_u is the ultimate bending moment, and k_m and k_u are the maximum and the ultimate stiffness, respectively. The index is formulated to start at zero in the absence of damage and to gradually increase to a maximum value of 1.0 as the structure approaches its ultimate condition.

Colombo and Negro (2005) [14] defined a general damage index as the ratio between the initial and the ultimate resistance capacity of RC elements.

$$DI_{\text{C-N}} = 1 - \left[\left(1 - \frac{\vartheta_m}{\vartheta_u}\right)^{\frac{1}{\beta_1}} \cdot 0.5 \left(1 - \tanh\left(\beta_2 \frac{\int dE}{E_u^*} - \pi\right)\right) \cdot e^{-\beta_3 \frac{\int dE}{E_u^*}} \right] \tag{14}$$

where $\beta_1 = \beta_3 = 0.1$, $\beta_2 = 2.4$, ϑ_m is the maximum rotation, ϑ_u is the ultimate rotation and E_u^* is a parameter that considers the dissipated energy.

Rodriguez and Padilla (2009) [15] proposed the following index considering using earthquake records which did not result in building collapse:

$$DI_{\text{R-P}} = \frac{E_h}{E_\lambda} \tag{15}$$

in which the energy absorbed in elastic system is

$$E_\lambda = k_\theta \theta_c^2 \tag{16}$$

where, for a single degree of freedom (SDOF), E_h is the hysteretic energy, k_θ is the elastic energy absorbed by SDOF system while it achieves $\theta = \pm 1$, θ_c is the maximum drift ratio.

Ladinović et al. (2011) [16] suggested a damage index based on displacement history, hysteretic energy and plastic deformation, modifying the existing Park and Ang model [7] to enhance damage assessment accuracy.

$$DI_{\text{L-al}} = \frac{d_m - d_y}{d_u - d_y} + \alpha\beta \frac{E_h}{F_y(d_u - d_y)} \tag{17}$$

in which

$$\alpha = 1 - \frac{\mu_c}{\mu_{ac}} \tag{18}$$

where d_u is the ultimate displacement under monotonic loading, d_m is the maximum displacement experienced during the earthquake, d_y is the yield displacement, μ_c ($\mu_c = d_{c,m}/d_y$) is the cyclic ductility depending on the maximum cyclic displacement request $d_{c,m}$ pending a ground movement [17], μ_{ac} is the accumulative ductility depending on the total inelastic displacements, β is the coefficient introduced by Park and Ang [7] defined in Equation (6), E_h is the hysteretic energy.

Guo et al. (2016) [18] developed another implementation of the existing Park and Ang index [7], proposing a three-dimensional damage index to account for the biaxial effect due to earthquake events.

$$DI_{\text{G-al}} = (1-\beta)\,\mu_{\theta,m}^{-} + \beta\int \alpha_m \frac{dE_p}{E_{mon}} \tag{19}$$

where β is the weight factor of energy dissipation, $\mu_{\theta,m}^{-}$ is the maximum normalized rotation ductility factor, dE_p is the plastic energy dissipation increment, E_{mon} is the value of plastic energy dissipation due to the effect of monotonic loading at the failure limit of the structure member, α_m is the correction of the energy dissipation term.

The aforementioned damage indexes can be classified based on the parameters involved in their formulation, as listed in Table 1, or based on the required knowledge of the structure as represented in Table 2.

Table 1. Classification of the damage indexes based on the parameters involved in the formulation.

Parameter	Indexes
Stiffness	Lybas and Sozen [4]; Banon et al. [5]; Hwang and Scribner [7]; Wang and Shah-1st [10]; Di Pasquale and Cakmak [12]; Bracci [13]
Ductility	Banon et al. [5]; Banon and Veneziano [6]; Park and Ang [8]; Wang and Shah-2nd [10]; Powell and Allahabadi [11]; Bracci [13], Colombo and Negro [14]; Ladinović et al. [16]; Guo et al. [18]
Number of cycles	Hwang and Scribner [7]; Stephensen and Yao [9]; Wang and Shah [10]
Energy	Banon and Veneziano [6]; Park and Ang [8]; Colombo and Negro [14]; Rodriguez and Padilla [15]; Ladinović et al. [16]; Guo et al. [18]
Combined	Banon and Veneziano [6]; Hwang and Scribner [7], Park and Ang [8]; Wang and Shah-2nd [10]; Bracci [13]; Colombo and Negro [14]; Ladinović et al. [16]; Guo et al. [18]

Table 2. Classification of the damage indexes based on the level of knowledge required.

Level of Knowledge	Indexes
Dynamic properties	Lybas and Sozen [4]; Hwang and Scribner [7]; Stephensen and Yao [9]; Di Pasquale and Cakmak [12]
Structural details	Banon et al. [5]; Banon and Veneziano [6]; Park and Ang [8]; Wang and Shah-1st [10]; Wang and Shah-2nd [10]; Powell and Allahabadi [11]; Bracci [13], Colombo and Negro [14]; Rodriguez and Padilla [15]; Ladinović et al. [16]; Guo et al. [18]

More precisely, the level of knowledge in Table 2 refers to parameters obtained from dynamic identification methods or on construction details, materials and dimensions required to define ductility, displacements and ultimate rotations.

To ensure a meaningful comparison, integration into decision-making processes and consistent model calibration, it is important that all index values are within the same range. A review of the literature shows that each index typically operates within its own range, so rescaling is necessary for consistency. In this context, the previous indexes have been rescaled so that they lie between 0, for no damage, and 1, for collapse. The rescaled damage indexes in this section are denoted as DI_*. The Lybas and Sozen index is rescaled as follows:

$$DI_{L-S*} = \frac{C}{ID_0} - C \tag{20}$$

with

$$C = \frac{k_e}{k_u - k_e} \tag{21}$$

where k_e and k_u are the secant stiffness at yield and at collapse of the element, respectively.

The indexes proposed by Banon and Veneziano, Hwang and Scribner, Park and Ang, Stephensen and Yao and Wang and Shah (first formulation) can be rescaled as follows:

$$DI_* = \frac{DI_0}{DI_u - DI_y} - \frac{DI_y}{DI_u - DI_y} \tag{22}$$

where DI_0 is the damage index calculated according to the original definition, DI_y is the damage index calculated at yield and DI_u is the damage index calculated at ultimate conditions.

The Wang and Shah index (second formulation) can be rescaled through the cyclic-loading parameter β as follows:

$$\beta_n = \frac{\beta_0}{\beta_u - \beta_y} - \frac{\beta_y}{\beta_u - \beta_y} \tag{23}$$

where β_0, β_y and β_u are the coefficients calculated according to the original definition, at yield and at ultimate conditions, respectively.

A graphical example of the scaling process is shown in Figure 1, where EDP stands for Engineering Demand Parameter and represents general structural response metrics used to estimate the extent of damage to structural components and systems, e.g., inter-story drift and element rotation. The indexes not mentioned do not need to be rescaled because they are already in the range from 0 to 1.

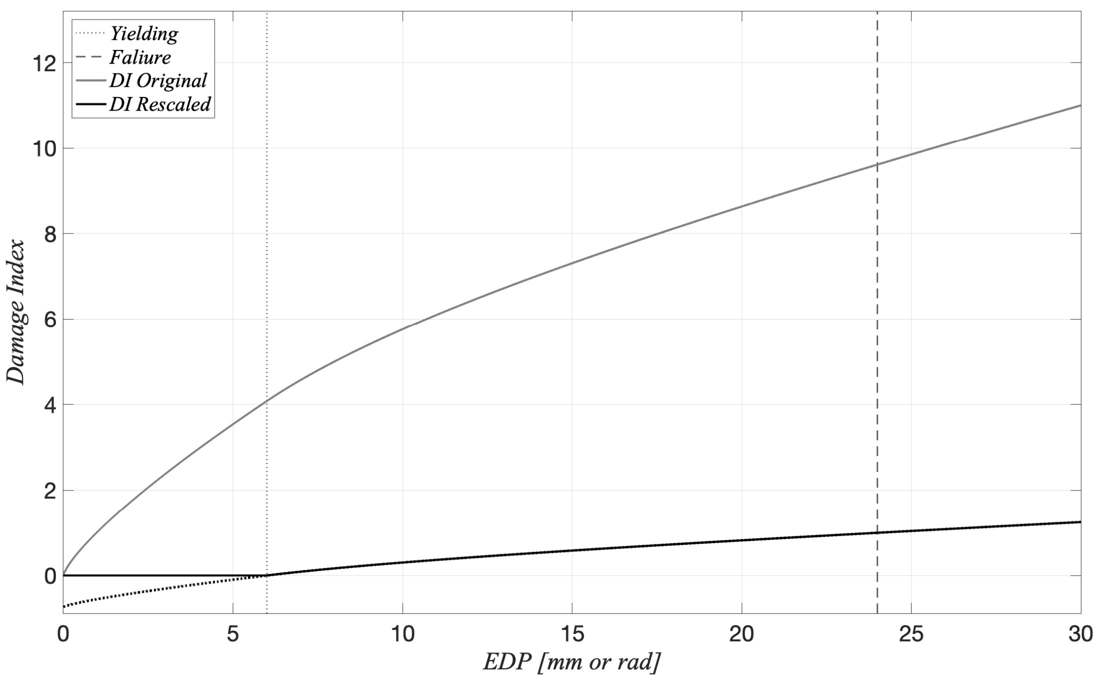

Figure 1. Example of rescaling for the Banon and Veneziano [6] index.

Since only Di Pasquale and Cakmak refer to the whole structure, the other indexes, referring to single structural elements, should be combined to obtain a global index. For this purpose, a method based on the weighted average of the indexes assessed for each element can be used. This approach considers the dissipated energy of each element: first, an index is computed to reflect the global damage state at each building level (Dlevel), then, such indexes are combined to obtain a global damage index (Dbuilding). The formulation of the indexes is

$$D_{level} = \frac{\sum_{i=1}^{n} D_i E_i}{\sum_{i=1}^{n} E_i} \quad (24)$$

$$D_{building} = \frac{\sum_{j=1}^{N} D_{level,j} E_{level,j}}{\sum_{j=1}^{N} E_{level,j}} \quad (25)$$

where D_i is the local damage index of the i-th structural element, n is the number of structural elements per building level, N is the total number of building levels, E_i is the energy dissipated by the i-th element and Elevel, j is the dissipated energy of the j-th level, the latter assessed as the sum of the dissipated energy of the structural elements belonging to the j-th level.

3. Damage Indexes Effectiveness

The efficiency of damage indexes in predicting and assessing the level of damage in an RC structure is evaluated using a reference case study in three different structural configurations, in particular:

1. An existing RC-frame building representative of a typical post-World War II construction (EX_MRF) designed for gravity load only;
2. A seismic code-conforming RC Moment-Resisting Frame structure (CC_MRF);
3. A seismic code-conforming RC wall building (CC_W).

For each configuration, the bare frame (BF) and the infilled frame (IF) configurations are considered to highlight the strengths and weaknesses of the damage indexes both with and without the interaction of infill panels.

3.1. Considered Case Study

The reference case study is a four-storey RC residential building in L'Aquila (AQ) (an area of high seismicity in Italy). It has a rectangular floor plan (21.05 m × 11.45 m). The first floor is 3.40 m high, while the inter-floor height for the rest of the building is 3.05 m (Figure 2). The one-way beam and block flooring system consists of RC beams and hollow bricks with a 5 cm thick RC overlay. The floor spans along the X-axis. The longitudinal and internal transverse RC beams are 25 cm deep; the depth of the transverse beams and edge beams varies depending on the configuration under consideration. The infill panels of the perimetral frame consist of two layers of hollow bricks (12 cm + 12 cm).

Concrete and steel materials with the following mechanical properties are considered as concrete C25/30 (f_{ck} = 25 N/mm^2, f_{cd} = 14.2 N/mm^2) and steel B450C (f_{yk} = 450 N/mm^2, f_{yd} = 391 N/mm^2). The existing building was designed for gravity loads only, whereas for the code-compliant cases, seismic actions were also considered. The applied loads are listed in Table 3.

Table 3. Permanent and live load applied to the structure (in kN/m^2). The infill load takes into account 15% of opening. Note: G refers to dead loads while Q for live loads.

Load	G_1-Floor and Roof	G_2-Floor	Q-Floor	G2-Roof	Q-Roof (Snow)	G2-Staircase	Q-Staircase	G2-Infill
Value	3.20	3.10	2.00	1.60	2.18	0.80	4.00	3.50

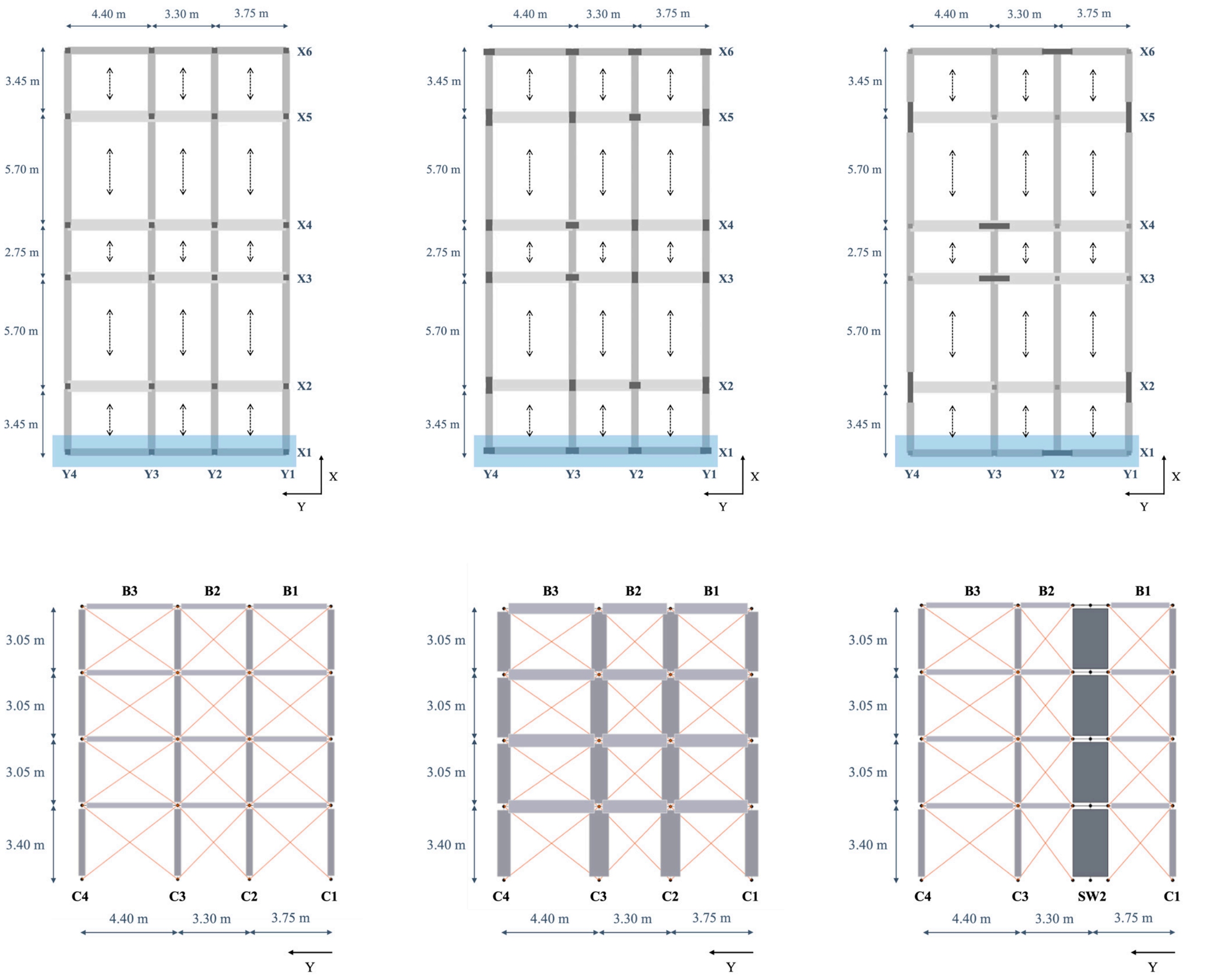

(**a**) (**b**) (**c**)

Figure 2. Reference plan and frontal view of the perimetral frame for (**a**) the existing structure (EX_MRF), (**b**) code-conforming moment-resisting frame (CC_MRF) and (**c**) code-conforming wall (CC_W).

For an initial assessment and development of methods and indicators that can accurately represent the state of the building after a seismic event, a 2D frame was extracted and considered for performing non-linear dynamic analysis: frame X1 highlighted in Figure 2. A planar frame analysis helps to avoid the influence of torsional phenomena on the interpretation of the damage indexes.

3.2. Numerical Modeling

For the numerical analyses, two finite element models have been developed. For the design phase, elastic models were developed with the software Midas GEN v.1.1 [19] and response spectrum analyses were conducted. For the performance assessment phase, non-linear models were developed with the software Opensees [20] and non-linear response history analyses were conducted.

For the response spectrum analyses, RC elements were modeled as *beam*-type elements with flexural stiffness scale factors equal to 0.7 and 0.5 for columns and beams, respectively. As for the shear walls, a stiffness scale factor equal to 0.7 was considered and the beam-to-shear wall connection was simulated by rigid elements linking the wall centroid to adjacent beams. Columns and shear walls were fixed at the base. Only the bare frame configuration (BF) was considered and masonry infill panels were accounted for only in terms of mass. The details of the frame cross-sections resulting from the design are listed in Tables 4–7.

Table 4. Geometrical properties and reinforcement details of beams and columns for the EX_MRF building.

ID	Element Type	Storey	Cross-Section (mm)	Longitudinal Reinforcement	Stirrups
C1-C2-C3-C4	Column	All	300 × 300	8ϕ14	ϕ10/200
B1-B2-B3 (i and j)	Beam	All	400 × 250	4ϕ14 top 4ϕ14 bot	ϕ10/200

Table 5. Geometrical properties and reinforcement details of beams and columns for the CC_MRF building.

ID	Element Type	Storey	Cross-Section (mm)	Longitudinal Reinforcement	Stirrups
C1-C4	Column	1	700 × 350	20ϕ24	3bϕ10/100
C2-C3	Column	1	900 × 350	26ϕ24	3bϕ10/75
C1-C4	Column	2, 3	600 × 350	18ϕ24	3bϕ10/100
C2-C3	Column	2, 3	800 × 350	22ϕ24	3bϕ10/75
C1-C4	Column	4	600 × 350	18ϕ24	3bϕ10/100
C2-C3	Column	4	700 × 350	20ϕ24	3bϕ10/100
B1-B2-B3 (i and j)	Beam	1, 2	350 × 600	6ϕ20 top 5ϕ20 bot	3bϕ10/100
B1-B2-B3 (i and j)	Beam	3, 4	350 × 500	6ϕ16 top 6ϕ16 bot	3bϕ10/100

Table 6. Geometrical properties and reinforcement details of beams and columns for the CC_W building.

ID	Element Type	Storey	Cross-Section (mm)	Longitudinal reinforcement	Stirrups
C1-C3-C4	Column	All	250 × 250	8ϕ16	ϕ8/90
B1-B2-B3 (i and j)	Beam	All	400 × 250	4ϕ16 top 4ϕ16 bot	4bϕ8/90

Table 7. Geometrical properties and reinforcement details of shear walls for the CC_W building.

ID	Element Type	Storey	Cross-Section [mm]	L_c [mm]	Reinforcement in L_c	Reinforcement in L_w	Stirrups
SW2	Shear wall	1	1600 × 300	600	20ϕ18	8ϕ10	ϕ10/100
SW2	Shear wall	2	1600 × 300	600	20ϕ16	8ϕ10	ϕ10/150
SW2	Shear wall	3	1600 × 300	600	20ϕ14	8ϕ10	ϕ10/150
SW2	Shear wall	4	1600 × 300	600	20ϕ12	8ϕ10	ϕ10/150

After completing the design phase, the final cross-section, the amount of longitudinal and transverse reinforcement, and the axial load in seismic condition were used to define the non-linear behavior of the structure. Two non-linear models were defined for each building configuration: the bare frame (BF) model, where only the infill mass is considered, and the infill frame (IF) model, which considers the contribution of the infills with an equivalent compression-only strut. Lumped plastic hinges were introduced to capture the non-linear behavior with the PeakOriented hysteretic model developed by Ibarra–Medina–Krawinkler (IMK) [21] (Figure 3a). Such hinges were applied by means of *zeroLength* elements in the end sections of the elements, while the inner part of the member was modeled with *ElasticBeamColumn* elastic frame elements.

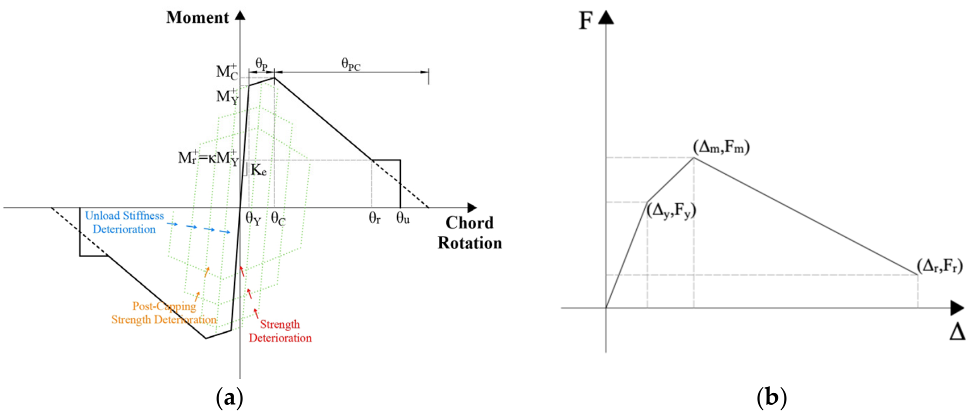

Figure 3. (**a**) Modified Ibarra–Medina–Krawinkler deterioration model (image from [20]) and (**b**) masonry infills backbone curve.

The infill panels were modeled as compression-only diagonal struts whose backbone curve values were derived from Decanini et al. [22] and adapted according to available experimental tests [23,24] and on the masonry properties defined by Hak et al. [25]. An example of the backbone curve is represented in Figure 3b whose values for a typical 30 cm thick infill panel with 2.65 m × 4.15 m dimensions are Δ_y, F_y (0.30%, 388 kN), Δ_m, F_m (0.50%, 485 kN) and Δ_m, F_m (1.86%, 0 kN).

For the non-linear assessment, Multi-Stripe Analyses (MSA) were conducted. MSA is a method that enables the evaluation of the seismic behavior of structures under earthquake scenarios with increasing intensity measures (IM) of ground motion. This method stems from the work of Cornell et al. [26] and aims to calculate the distributions of one or more Engineering Demand Parameter for several scenarios of ground motion records represented by an intensity measure, herein represented by the elastic spectral acceleration, $S_a(T_j)$, at the fundamental period of vibration of the building, T_j.

Ten intensity measure levels (IMLs) were considered for each building type and configuration (i.e., BF, IF) corresponding to return periods of 10, 50, 100, 250, 500, 1000, 2500, 5000, 10,000 and 100,000 years for the site of L'Aquila (high seismicity area in Italy), with a soil category C [27]. For each intensity level, 20 different ground motions were selected from the DPC-ReLUIS project and were used to evaluate the Engineering Demand Parameters (EDP) [28,29] adopting the conditional mean spectrum approach [30]. The conditioning periods at which the various spectra of the chosen ground motion converge to the spectral acceleration at each intensity level are reported in Table 8.

Table 8. Conditioning periods chosen for each configuration of the building.

Case Study	Building Fundamental Period (T_1) [s]	Selected Conditioning Period (T_j) [s]
Existing building (BF)	1.55	1.50
Existing building (IF)	0.27	0.15
Code-conforming wall building (BF)	0.62	0.50
Code-conforming wall building (IF)	0.17	0.15
Code-conforming MRF building (BF)	0.56	0.50
Code-conforming MRF building (IF)	0.18	0.15

3.3. MSA Results

In this study, the results of the MSA are used to calculate the values of the considered damage indexes and to assess their effectiveness and reliability compared to various damage scenarios and performance levels, selected according to the DPC-ReLUIS project [28,29] and Eurocode 8 [27]: Usability Preventing Damage (UPD), Life Safety (LS), Collapse Prevention (CP) and Global Collapse (GC). Table 9 lists the limit states and the corresponding structural conditions.

Table 9. Considered limit states and performance levels.

Limit State/Performance Level	Description
Usability Preventing Damage (UPD)	Defined according to Eurocode 8: it aims to withstand a seismic action having a larger probability of occurrence than the design seismic action, without the occurrence of damage and the associated limitations of use, the costs of which would be disproportionately high in comparison with the costs of the structure itself.
Life Safety (LS)	Defined according to Eurocode 8: it aims to protect occupants from serious injury and to allow safe evacuation. Although significant structural and non-structural damage may occur, the critical load-bearing elements of the building must remain intact to prevent complete structural failure. Herein considered when the inter-story drift ratio reaches a value of 2%.
Collapse Prevention (CP)	Defined according to Eurocode 8: it represents the stage at which the structure is severely damaged, with large permanent drifts, but retains its vertical load-bearing capacity and most of the ancillary components, if any, have collapsed. Herein considered when the top displacement reaches the value corresponding to a 20% degradation of the maximum base shear obtained from a non-linear static, pushover, analysis.
Global Collapse (GC)	Defined according to Eurocode 8: it represents the stage at which the structure could be considered to have collapsed. Herein considered when the top displacement reaches the value corresponding to a 50% degradation of the maximum base shear obtained from a non-linear static, pushover, analysis.

Figure 4a provides an example of the results obtained from the analysis as diagrams showing the damage index values as a function of the spectral acceleration. The complete graphical representation is reported in Appendix A for different building configurations.

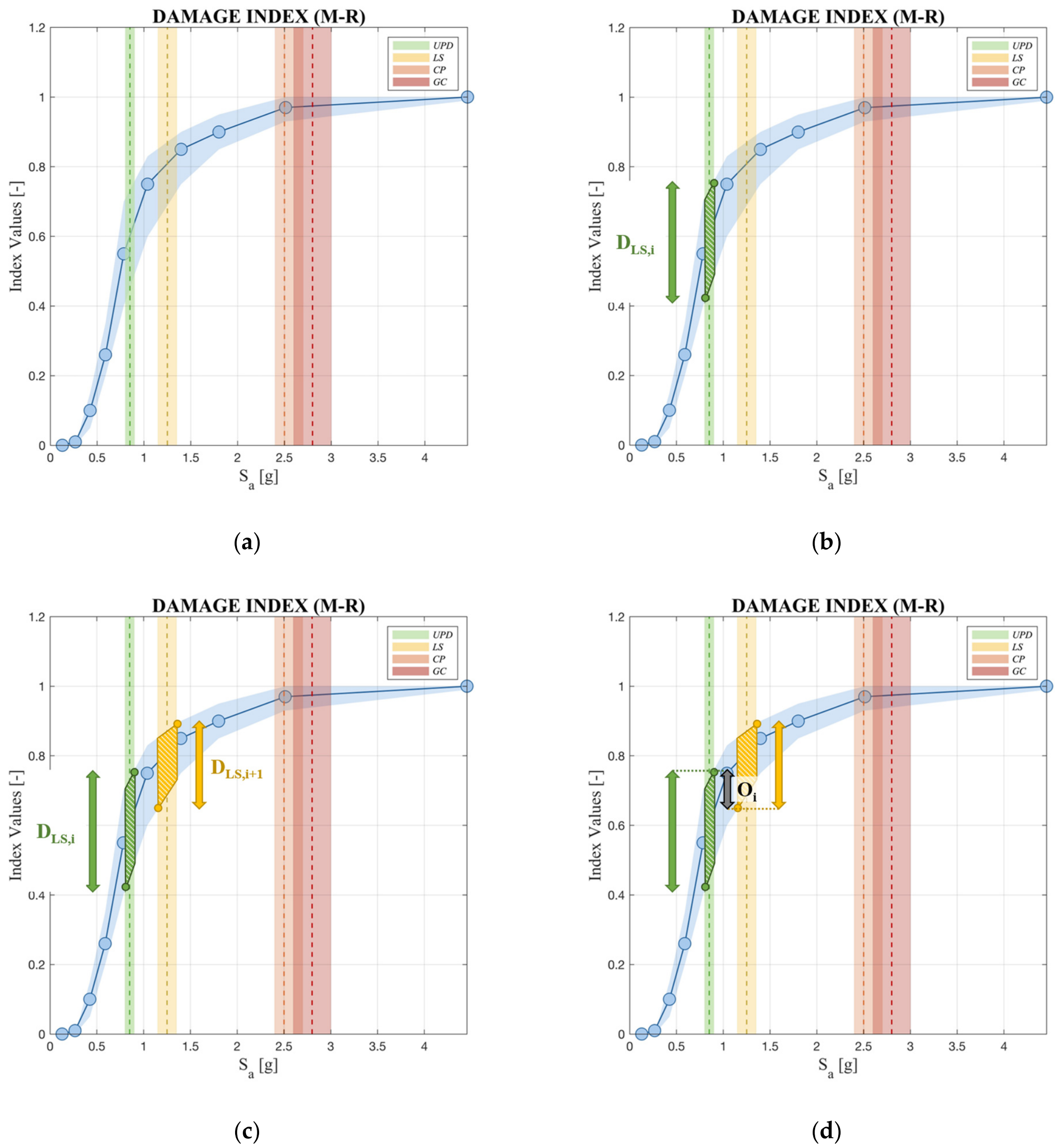

Figure 4. (**a**) Example of the computation of the damage index using the M-R approach. (**b**) Graphical representation of the dispersion (D) for a generic limit state i. (**c**) Visualization of the dispersion $D_{LS,i}$ and $D_{LS,i+1}$ for consecutive limit states. (**d**) Representation of the overlap (O_i) between two consecutive limit states-performance levels.

In Figure 4a, the solid blue line and the blue circles show the median value of the damage indexes calculated over the 10 IM levels. This provides a representation of the central tendency of the damage indexes. The light blue shaded area shows the interquartile range (25th to 75th percentile), which illustrates the variability of the index, with wider ranges reflecting greater uncertainty. The vertically shaded areas correspond to the defined performance levels: UPD (green), LS (orange), CP (red) and GC (dark red). The width of these areas represents the interquartile range of the performance levels while the dashed vertical line represents the median value. This representation highlights the damage index value dispersion within the same intensity level and offers a clear view of the variability and robustness of the indicators. Herein, only the damage indexes calculated starting from the moment-rotation values of the RC elements are represented. Similar results are obtained from the damage indexes calculated starting from the floor shear-interstory drift values.

In order to better assess the efficiency of each damage index, specific parameters are introduced to highlight their accuracy in detecting damage while minimizing the overlap between the limit states and reducing the dispersion of the data. The dispersion (D) measures the variability of the values within a given limit state-performance level by calculating the difference between the maximum and minimum values in the interquartile range and provides an indication of the accuracy of the data. This is shown graphically in Figure 4b,c. The overlap parameter (O) evaluates the potential overlap between consecutive limit states and indicates the risk of misinterpretation of the damage levels and the uncertainty in distinguishing between them. Figure 4d graphically represents this parameter, which reflects the precision and reliability of the damage indexes in the assessment of seismic performance.

Tables 10 and 11 summarize the results of damage index curves plotted in Appendix A, where the damage index values are plotted as a function of the spectral acceleration. The comparison of the individual indexes aims to provide a clear evaluation of the efficiency of the damage indicators for the different structural systems in both bare and infilled frame configurations. The results for each building configuration are reported in Appendix B. In these tables, indexes are cited as L-S for Lybas and Sozen (1977) [4], FDR for Banon et al. (1977) [5], B-V for Banon and Veneziano (1982) [6], P-A for Park and Ang (1985) [8], W-S-1 for Wang and Shah (first formulation (1987)) [10] and P-Al for Powel and Allahabadi (1988) [11]. When analyzing the damage indexes for different building typologies (as also reported graphically in Appendix A), especially in the bare frame configuration, the indexes show strong capabilities in detecting and quantifying damage. In this configuration, the indexes exhibit remarkable uniformity in damage quantification, with overlaps O1 and O2 equal to zero for all damage indexes (except for Lybas and Sozen) and low dispersion values (D). This underlines their potential for effective "real-time" damage detection in BF configurations for all building types. Conversely, the performance of these indexes decreases when evaluating infilled structures. While all indexes successfully track incremental damage with increasing intensity, they exhibit greater variability, with larger dispersion values (D) and increased sensitivity to building typology. This greater heterogeneity leads to a significant overlap between the different damage states, with higher values already from O_2 for LS-CP. These overlaps reduce the effectiveness of the damage indexes and limit their applicability for the reliable prediction of damage in infilled structures.

In particular, in the bare-frame configuration for existing MRF and SW buildings, the L-S and P-A indexes show high efficiency for the UPD and LS limit states. They exhibit no overlap O1 and O2 and a low to medium dispersion, ranging from less than 5% for UPD to 25% for LS. However, for the CP and GC limit states, their efficiency decreases significantly due to a significant overlap (about 95%) and a larger dispersion of about 10% to 80%. Similarly, the B-V, W-S-1 and P-Al indexes show high efficiency for UPD for all building types, with a very good LS performance for frame systems. They show no overlap O1 and O2 and a low dispersion, ranging from 0% to 15% for existing and MRF buildings and up to 40% for LS in the shear wall configuration. On the other hand, their efficiency decreases for CP and GC due to overlaps of more than 95% and higher dispersion values of 10% to 40%, reflecting the trends observed for other indexes. Conversely, the FDR Banon index performs well for UPD as it has no overlap and very low dispersion. However, its efficiency decreases for LS, where the overlap O2 is between 5% and 20% with increasing dispersion. For CP and GC, the FDR index mirrors the trend of the other indexes, with lower efficiency due to significant overlap O3 and higher dispersion. Therefore, to improve the damage index performance, it is suggested to consider just an ultimate performance level, condensing CP and GC.

Table 10. Overview of the dispersion (D) of all damage indexes for each limit state for all the building configurations.

DISPERSION (D)																								
	EX_MRF_BF				**EX_MRF_IF**				**CC_MRF_BF**				**CC_MRF_IF**				**SW_MRF_BF**				**SW_MRF_IF**			
Index	**UPD** [%]	**LS** [%]	**CP** [%]	**GC** [%]	**UPD** [%]	**LS** [%]	**CP** [%]	**GC** [%]	**UPD** [%]	**LS** [%]	**CP** [%]	**GC** [%]	**UPD** [%]	**LS** [%]	**CP** [%]	**GC** [%]	**UPD** [%]	**LS** [%]	**CP** [%]	**GC** [%]	**UPD** [%]	**LS** [%]	**CP** [%]	**GC** [%]
L-S	4.2	9.0	6.9	7.0	27.6	71.0	8.4	5.4	0.0	23.4	12.5	12.6	23.4	41.8	37.0	44.9	9.9	12.8	5.7	5.1	58.6	29.5	8.8	9.2
FDR	20.6	4.4	7.3	7.3	6.4	75.3	19.3	12.5	0.0	14.0	23.4	23.4	19.2	32.9	56.9	62.7	6.6	36.1	20.7	18.3	21.9	52.5	44.0	44.5
B-V	0.9	14.4	11.3	9.6	12.3	68.4	2.0	1.3	0.0	7.2	40.7	32.8	1.5	23.7	91.2	94.4	0.2	40.4	43.0	37.9	1.5	56.9	71.4	71.8
P-A	0.0	25.1	43.0	44.8	13.2	73.3	14.1	9.1	0.0	4.7	66.2	81.9	1.4	18.1	93.2	95.1	0.3	24.1	49.0	45.8	7.3	60.2	75.5	75.8
W-S-1	1.9	11.0	20.4	17.1	3.9	125	48.0	31.0	0.0	7.4	23.9	20.7	21.0	27.3	63.9	68.6	1.4	39.3	28.2	25.2	8.4	55.5	50.1	50.7
P-Al	1.7	13.3	8.7	7.4	6.4	75.3	19.3	12.5	0.0	11.7	30.3	23.8	4.8	33.2	78.7	85.0	1.0	40.1	28.4	25.1	8.0	57.4	51.1	51.7

Table 11. Overview of the overlap (O) of all damage indexes for each limit state for all the building configurations.

OVERLAP (O)																		
	EX_MRF_BF			**EX_MRF_IF**			**CC_MRF_BF**			**CC_MRF_IF**			**SW_MRF_BF**			**SW_MRF_IF**		
Index	**UPD LS** [%]	**LS CP** [%]	**CP GC** [%]	**UPD LS** [%]	**LS CP** [%]	**CP GC** [%]	**UPD LS** [%]	**LS CP** [%]	**CP GC** [%]	**UPD LS** [%]	**LS CP** [%]	**CP GC** [%]	**UPD LS** [%]	**LS CP** [%]	**CP GC** [%]	**UPD LS** [%]	**LS CP** [%]	**CP GC** [%]
L-S	0.0	0.0	96.9	0.0	11.8	64.7	0.0	0.0	91.4	0.0	48.3	100	0.0	0.5	87.1	0.0	19.2	100
FDR	0.0	18.1	94.7	0.0	25.6	64.7	0.0	0.0	86.1	0.0	53.1	100	0.0	5.8	87.1	0.0	54.7	100
B-V	0.0	0.0	79.8	0.0	2.9	64.7	0.0	0.0	66.7	0.0	73.5	100	0.0	0.0	87.6	0.0	65.4	100
P-A	0.0	0.0	94.4	0.0	19.2	64.7	0.0	0.0	93.6	0.0	78.3	100	0.0	0.0	88.7	0.0	78.0	100
W-S-1	0.0	0.0	80.5	0.0	38.5	64.7	0.0	0.0	70.4	0.0	53.4	100	0.0	0.0	87.7	0.0	47.4	100
P-Al	0.0	0.0	80.1	0.0	25.6	64.7	0.0	0.0	65.5	0.0	61.0	100	0.0	0.0	87.6	0.0	47.7	100

In the case of infilled configurations, the FDR and W-S-1 indexes show a high efficiency in distinguishing damage related to UPD and LS for all building types. These indexes show no overlap O1 and a low to medium dispersion between 5% and 20%. However, their efficiency decreases for LS and CP due to significant overlap O2 between 25% and 55%, accompanied by an increased dispersion over 20%. The B-V and P-A indexes maintain their high efficiency for UPD, as they have no overlap O1 and scatter values between 1% and 15%. However, their reliability decreases for LS, CP and GC, with overlap O2 increasing from 5% to 80% and dispersion values increasing from 20% to 65%. Similarly, the P-AI index for UPD has a minimum dispersion from 5% to 10% and no overlap O1, but its efficiency decreases for LS, CP and GC due to a larger overlap O_2 ranging from 25% to 60% and a larger dispersion. Conversely, the L-S index shows reasonable efficiency but lower precision for UPD, with no overlap O_1 and dispersion values between 20% and 60%. For LS, CP and GC, its behavior mirrors the trend observed for the other indexes, with reliability decreasing at higher damage states due to greater overlap and scatter.

After analyzing the behavior of the damage indexes in the BF and IF configurations, the most appropriate index for each building configuration can be identified. For BF configurations in all analyzed building types, most of the indexes effectively detect damage without misinterpreting the LS and CP/GC states, except for the FDR-Banon index. Among these indexes, Lybas and Sozen's index proves to be the optimal choice for all BF configurations, as it consistently has lower dispersion values for the CP and GC limit states. As far as IF configurations are concerned, the FDR-Banon index is the most efficient index for the pre-code moment-resisting frame. This index has the lowest overlap between the LS and CP/GC limit states and one of the lowest dispersion values for the CP and GC limit states. In contrast, Lybas and Sozen's index proves to be the most effective choice for both the moment-resisting frame and the shear wall system for code-compliant buildings. It minimizes overlap and dispersion while optimizing calculation time, making it the preferred index for these configurations.

Although originally developed for structural RC elements, the evaluation of the efficiency and reliability of damage indexes in this study is extended to non-structural elements, such as masonry infills, which significantly affect repair costs after a seismic event. To achieve this, specific indexes are defined and tested to quantify the damage level of masonry infills. Among these, the index of Lybas and Sozen and the index of Powell and Allahabadi are selected as the most efficient and computationally effective options for calculating the damage level of masonry infills. In addition, a new dissipated energy-based index is introduced, based on the ratio between the area under the trilinear curve of the infill panel up to the point reached during the analysis and the total area under the trilinear curve.

The effectiveness and adaptability of the analyzed infill indexes are evaluated by comparing the median values that each index assumes in each infill during the analyzed intensity measures (IMs) in the Multiple Stripe Analysis. Three threshold values are determined, corresponding respectively to the elastic limit of the infill, the maximum capacity of the infill and the failure of the infill. These three thresholds define four states of damage for the infill: the elastic and uncracked phase, the cracked phase, the softening phase and, finally, failure. These are shown respectively with green, yellow, light red and dark red color codes. The stage of each infill is defined based on the median value that each index assumes for the infill under investigation during the analyzed strip.

The results showed that all three indexes were able to capture the growth and increase of infill damage in all building configurations studied, making these indexes an effective tool for detecting damage to closure panels regardless of building typology. In particular, the P-Al index and the energy-based index are particularly effective in progressively assessing damage to these elements. Conversely, the L-S index could potentially lead to an underestimation of damage, especially if it is close to the elastic limit. An example of the damage progression in infills of the shear wall building is represented in Figure 5.

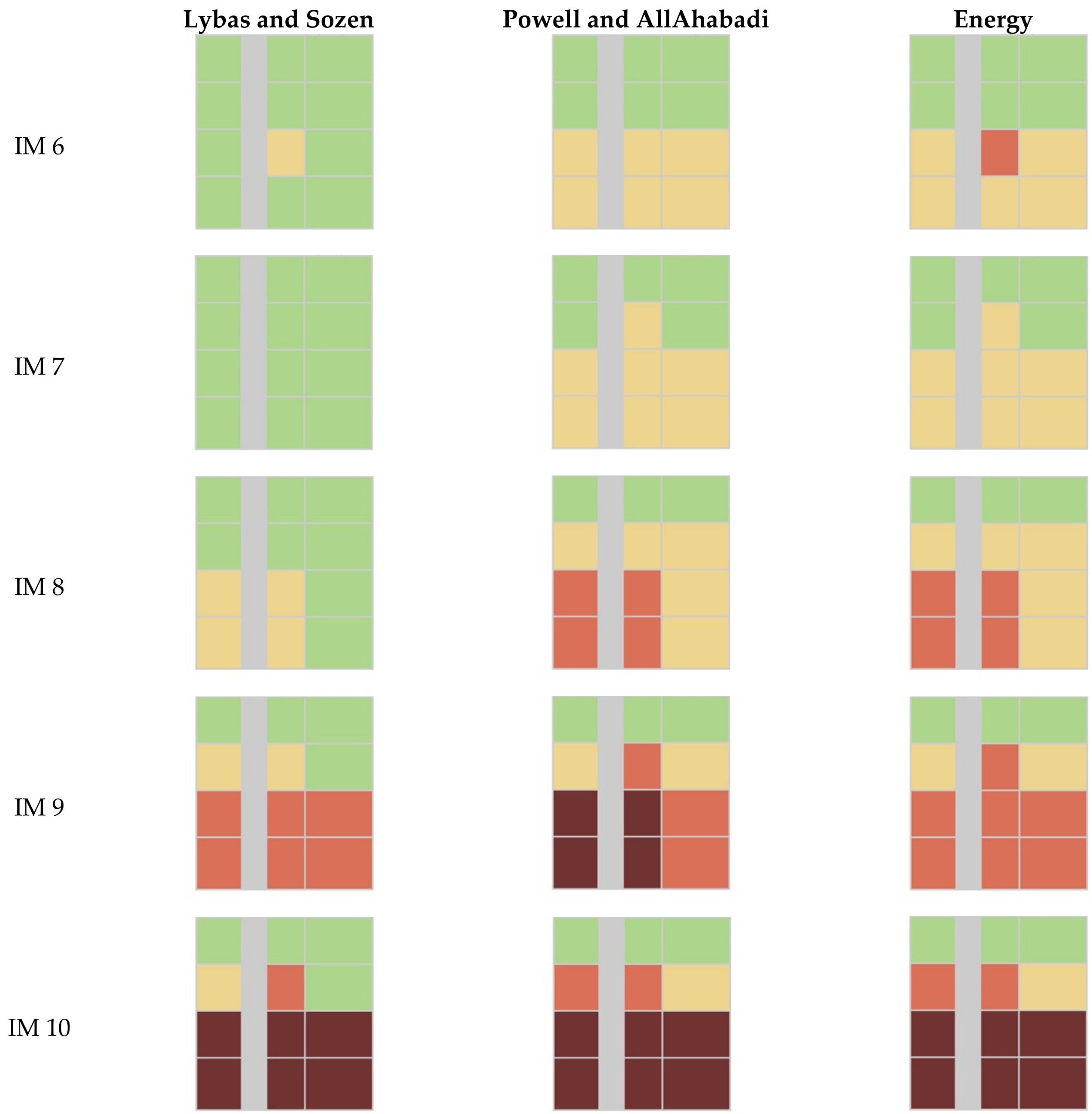

Figure 5. Visualization of the progression of damage through Lybas and Sozen, Powell and Allahabadi and energy-based indexes for the CC_W_IF building. Note: the green, yellow, orange and dark red refer to the UPD, LS, CP and GC performance levels, respectively.

4. Conclusions

The detection and quantification of damage to reinforced concrete (RC) buildings is an important area of research driven by the recurrent and significant damage caused by earthquakes over the years and by the possibility of creating digital twins of existing buildings to directly assess damage after earthquakes. The aim of this work was to evaluate the effectiveness and reliability of different damage indexes to ultimately identify tools that can improve seismic risk assessment and demonstrate their potential applicability for digital twins of RC buildings, which is crucial for post-earthquake assessment.

First, a comprehensive literature review was conducted to examine damage indexes that have been developed and used in the past. Notable examples include the indexes proposed by Lybas and Sozen, Park and Ang, and Banon and Veneziano. Following the literature review, the study focused on evaluating the efficiency of selected damage indexes for an RC reference building. This building was analyzed under three different structural configurations: an existing gravity-only moment-resisting frame, a code-compliant moment-resisting frame, and a code-compliant shear wall system that accounts for seismic loading. In addition, both the bare frame and the masonry infilled frame conditions were analyzed for each building configuration. The seismic performance of the building was thoroughly evaluated using Multi-Stripe Analyses, which allowed for a detailed assessment across different intensity levels.

The study shows which indexes are most suitable for certain situations and which are less effective. It is worth noting that cycle-related indexes were not considered as they cannot be directly compared to other indexes unless a rescaling approach is provided. This limitation results from their mathematical formulation. In particular, by summing the damage from each hysteretic cycle, the index value can exceed 1, so a direct comparison with other indexes—which are typically defined between 0 (no damage) and 1 (collapse)—is not possible. In the case of cycle-related indicators, specific performance values must be defined for each index.

In BF configurations, most indexes effectively detect damage without misinterpreting the LS and CP/GC states, with the exception of the FDR-Banon index. Among these, Lybas and Sozen's index and Powell and Allahabadi's index have been found to be the optimal choice for all BF configurations, as they consistently have lower scatter values for the CP and GC limit states.

For the IF configurations, the FDR-Banon index proved to be the most efficient index for the pre-coded moment-resisting frame. This index has the lowest overlap between the LS and CP/GC limit states and one of the lowest scatter values for the CP and GC limit states. In contrast, Lybas and Sozen's index is the most effective choice for both moment-resisting frames and shear wall systems in code-compliant buildings. It minimizes overlap and scatter while optimizing calculation time, making it the preferred index for these configurations.

For non-structural elements, such as masonry infill, both the Lybas and Sozen index and the Powell and Allahabadi index proved to be the most efficient options for assessing the extent of damage. In addition, a new dissipated energy-based index was developed based on the ratio between the area under the trilinear curve of the infill panel up to the point reached during the analysis and the total area under the curve. The results show that all three indexes can capture the growth and increase in infill panel damage in all building configurations studied, making them effective tools for detecting damage to closure panels regardless of building typology. In particular, the Powell and Allahabadi index and the energy-based index are especially effective for the progressive assessment of damage to these elements, while the Lybas and Sozen index can lead to an underestimation of damage.

In general, the damage indexes proved to be very effective in detecting not only the presence of damage, but also its extent. Importantly, the results of this study highlight the potential benefits of applying damage indexes in advanced monitoring and assessment systems, particularly in digital twin systems and sensor-based applications.

Damage indexes can improve real-time assessment of seismic damage and decision making after seismic events, which is an important aspect of engineering practice. In particular, seismic design should consider structural safety together with optimization of available resources and prioritization of actions. The use of damage indexes to quickly identify damage and vulnerabilities enables more informed decisions leading to a more efficient use of resources in post-earthquake rehabilitation. In addition, the use of damage indexes could promote a more integrated and systematic approach to resource allocation for seismic rehabilitation measures by moving from assessing the vulnerability of individual buildings to a damage index ranking of the different buildings in the urban context.

Author Contributions: Conceptualization, L.D., M.G., S.L. and A.B.; methodology, L.D. and A.B.; software, L.D.; validation, L.D., M.G., S.L. and A.B.; formal analysis, L.D.; writing—original draft preparation, M.G.; writing—review and editing, L.D., M.G., S.L. and A.B.; visualization, L.D., M.G., S.L. and A.B.; supervision, A.B. All authors have read and agreed to the published version of the manuscript.

Funding: This research received no external funding.

Institutional Review Board Statement: Not applicable.

Informed Consent Statement: Not applicable.

Data Availability Statement: The raw data supporting the conclusions of this article will be made available by the authors on request.

Acknowledgments: The studies presented here were partially carried out as part of the activities envisaged by the Agreement between the Italian Department of Civil Protection (DPC) and the ReLUIS Consortium. The contents of this paper represent the authors' ideas and do not necessarily correspond to the official opinion and policies of DPC.

Conflicts of Interest: The authors declare no conflicts of interest.

Appendix A

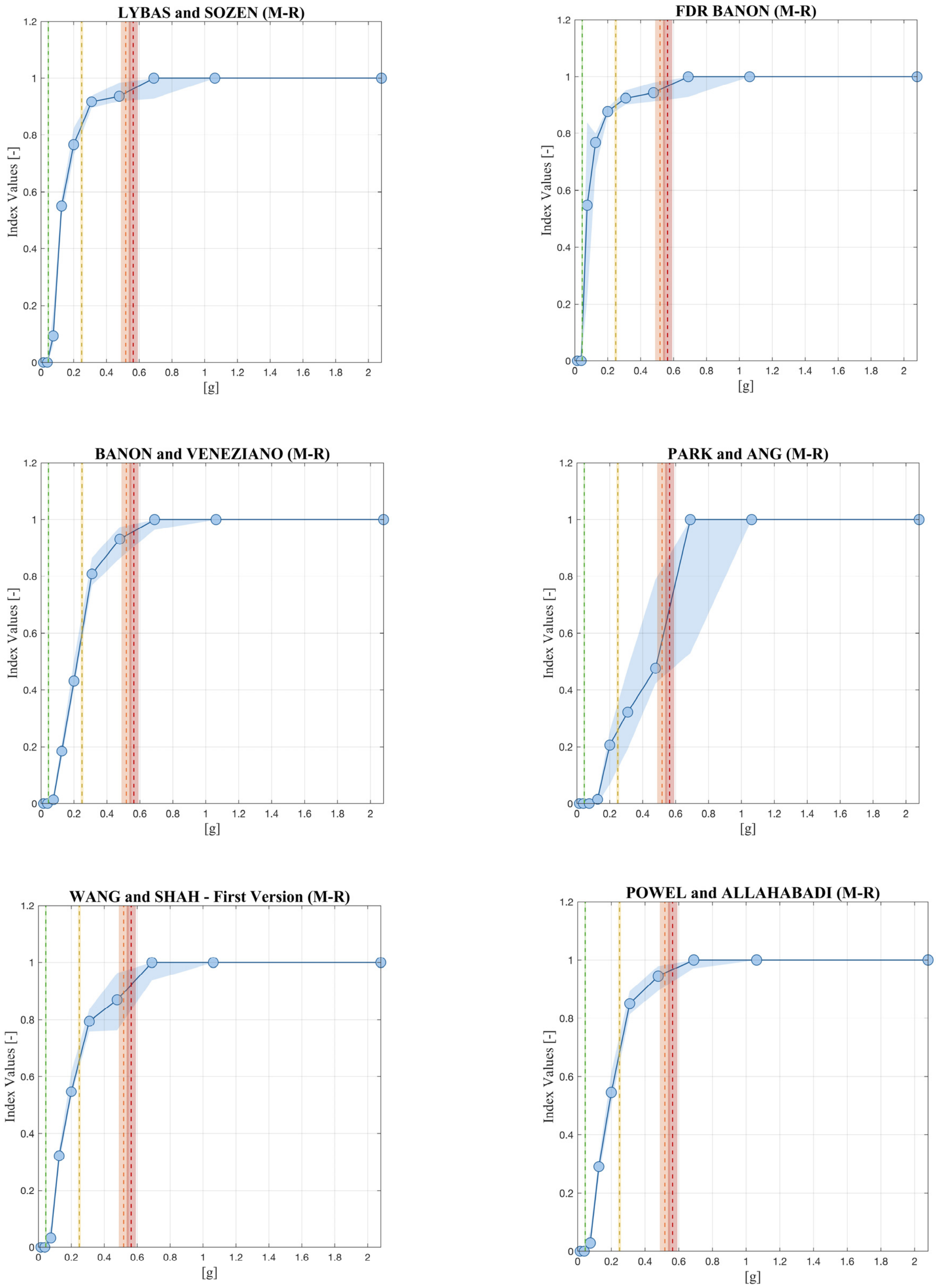

Figure A1. Damage indexes for the existing RC frame building in the bare frame configuration (EX_MRF_BF). Note: the green, yellow, orange and red refer to the UPD, LS, CP and GC performance levels, respectively.

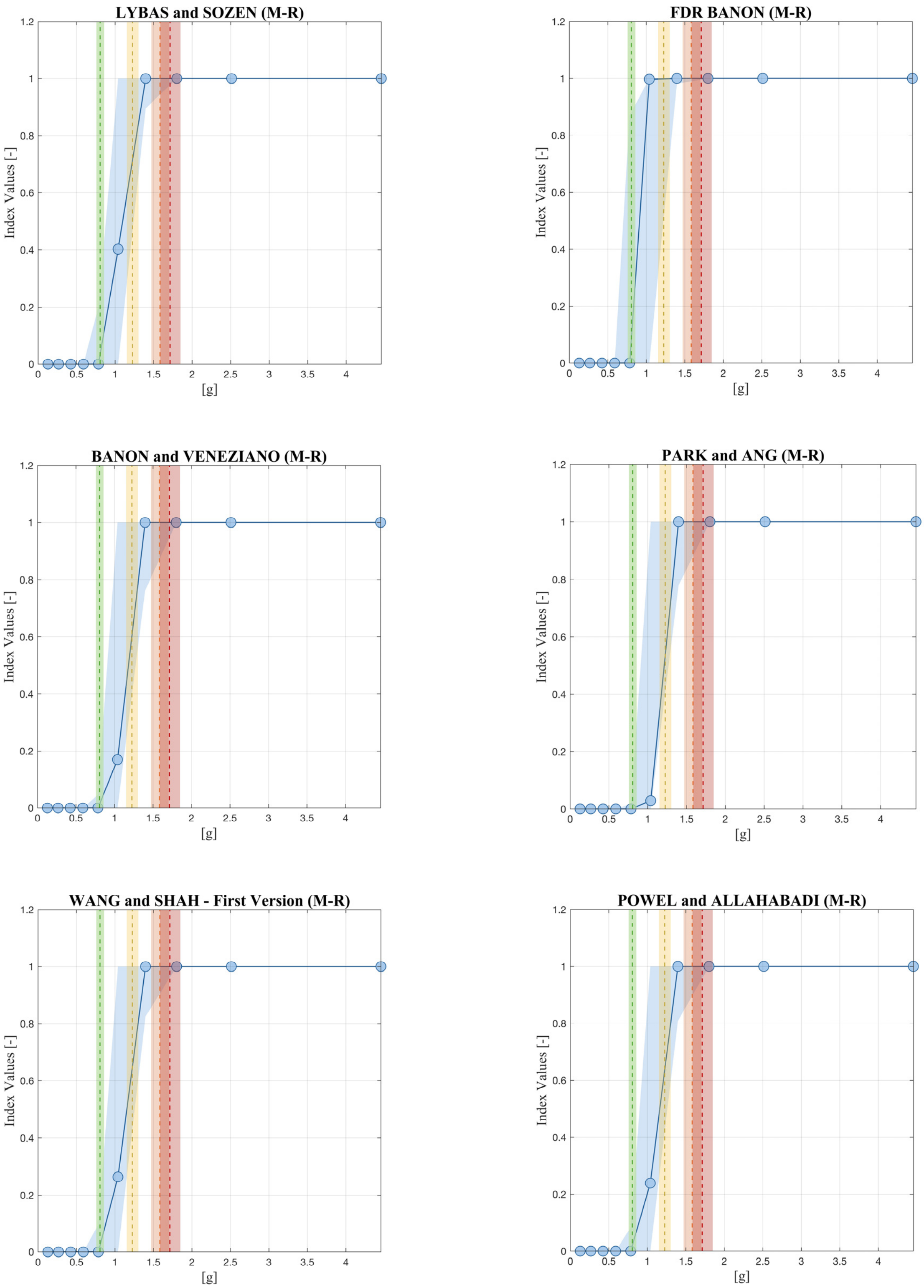

Figure A2. Damage indexes for the existing RC frame building in the infilled frame configuration (EX_MRF_IF). Note: the green, yellow, orange and red refer to the UPD, LS, CP and GC performance levels, respectively.

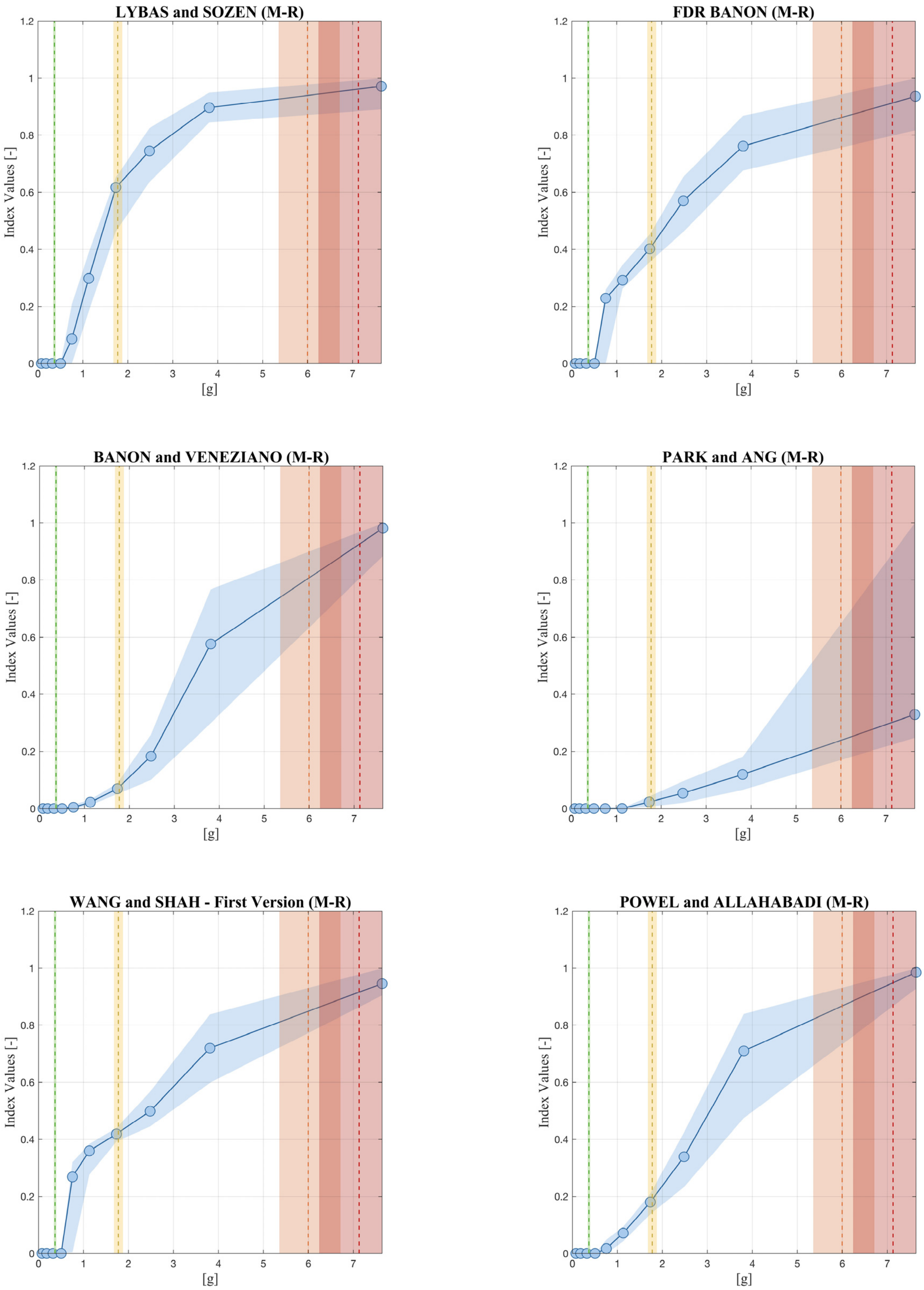

Figure A3. Damage indexes for the code-conforming MRF building in the bare frame configuration (CC_MRF_BF). Note: the green, yellow, orange and red refer to the UPD, LS, CP and GC performance levels, respectively.

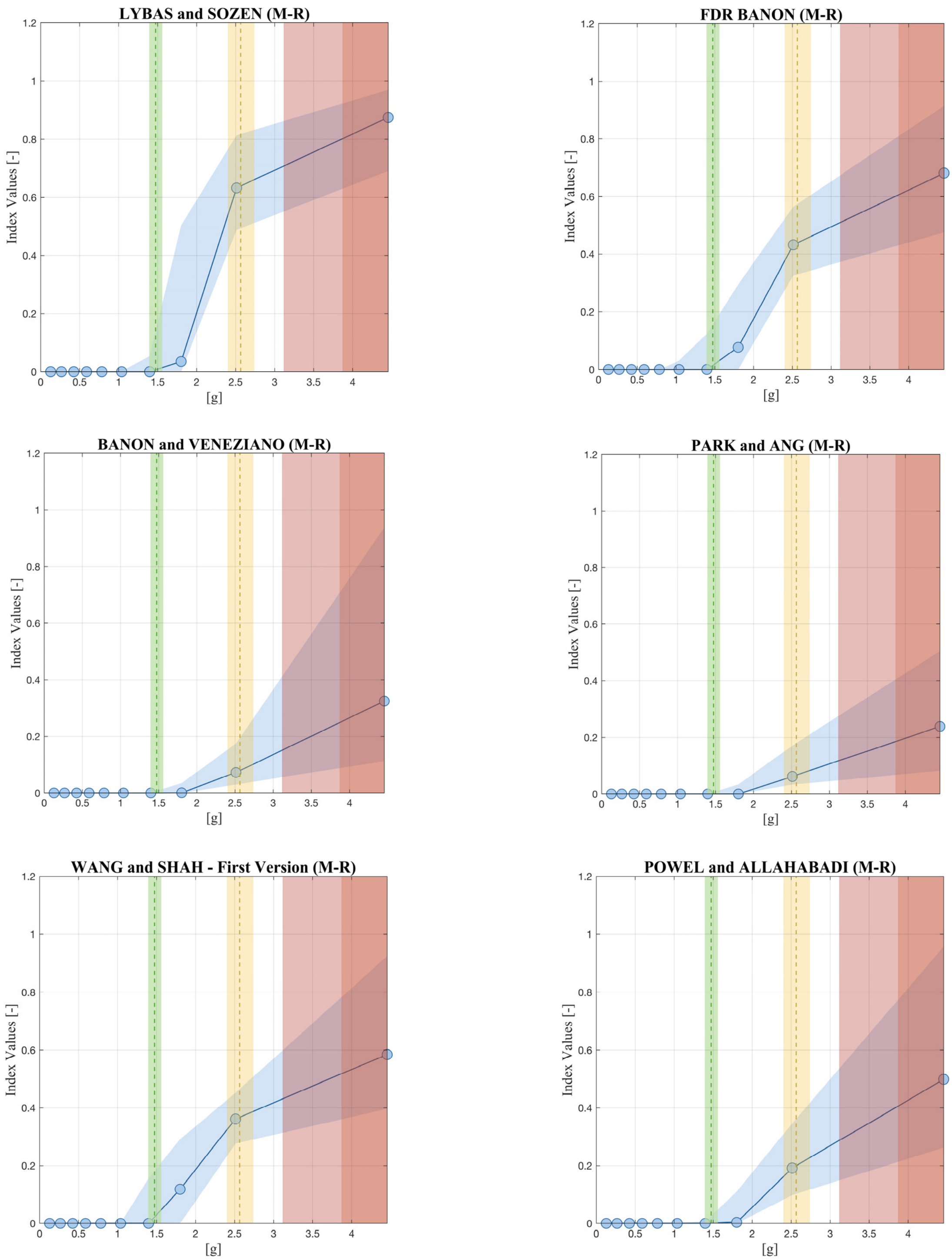

Figure A4. Damage indexes for the code-conforming MRF building in the infilled frame configuration (CC_MRF_IF). Note: the green, yellow, orange and red refer to the UPD, LS, CP and GC performance levels, respectively.

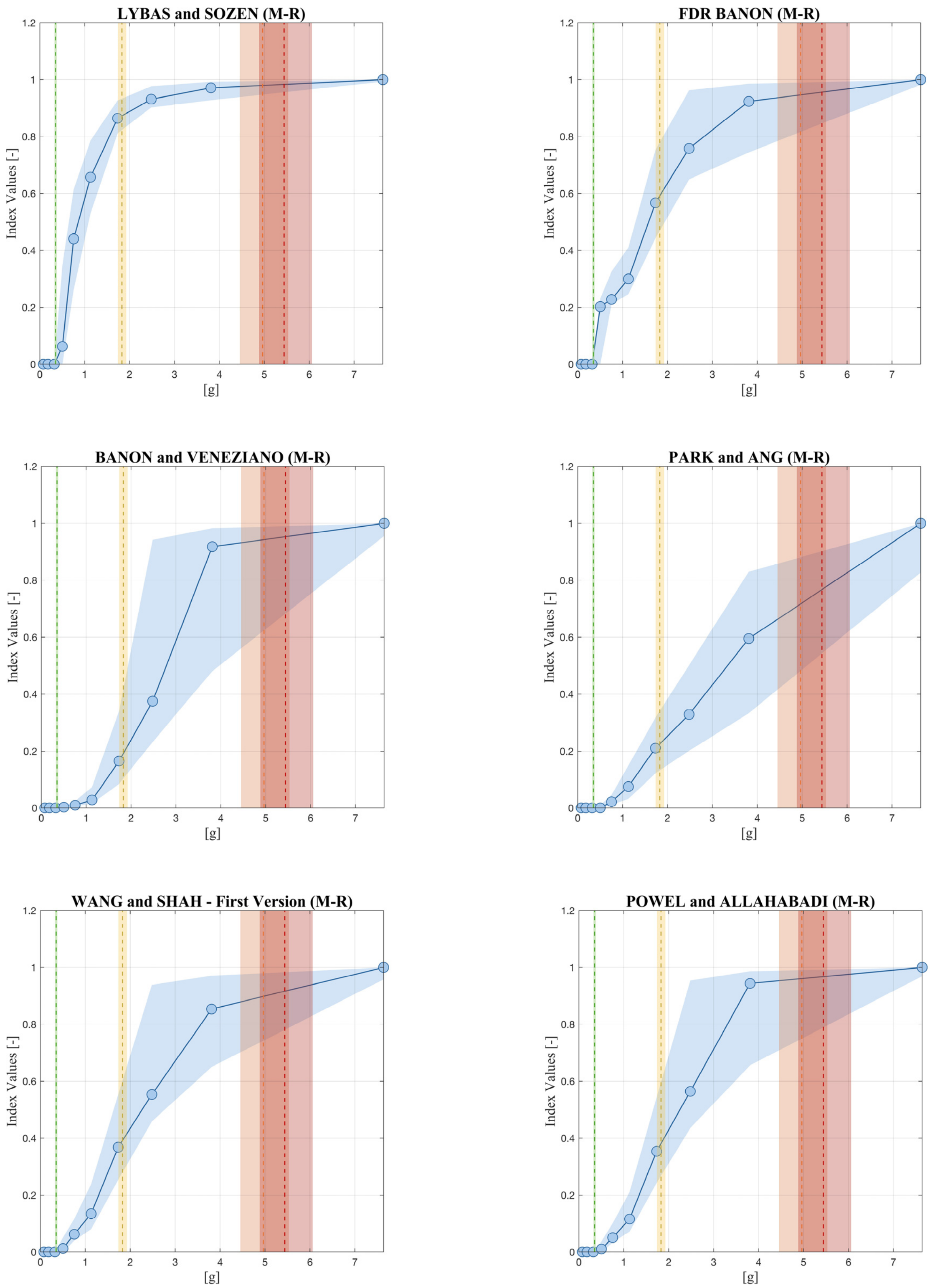

Figure A5. Damage indexes for the code-conforming SW building in the bare frame configuration (CC_W_BF). Note: the green, yellow, orange and red refer to the UPD, LS, CP and GC performance levels, respectively.

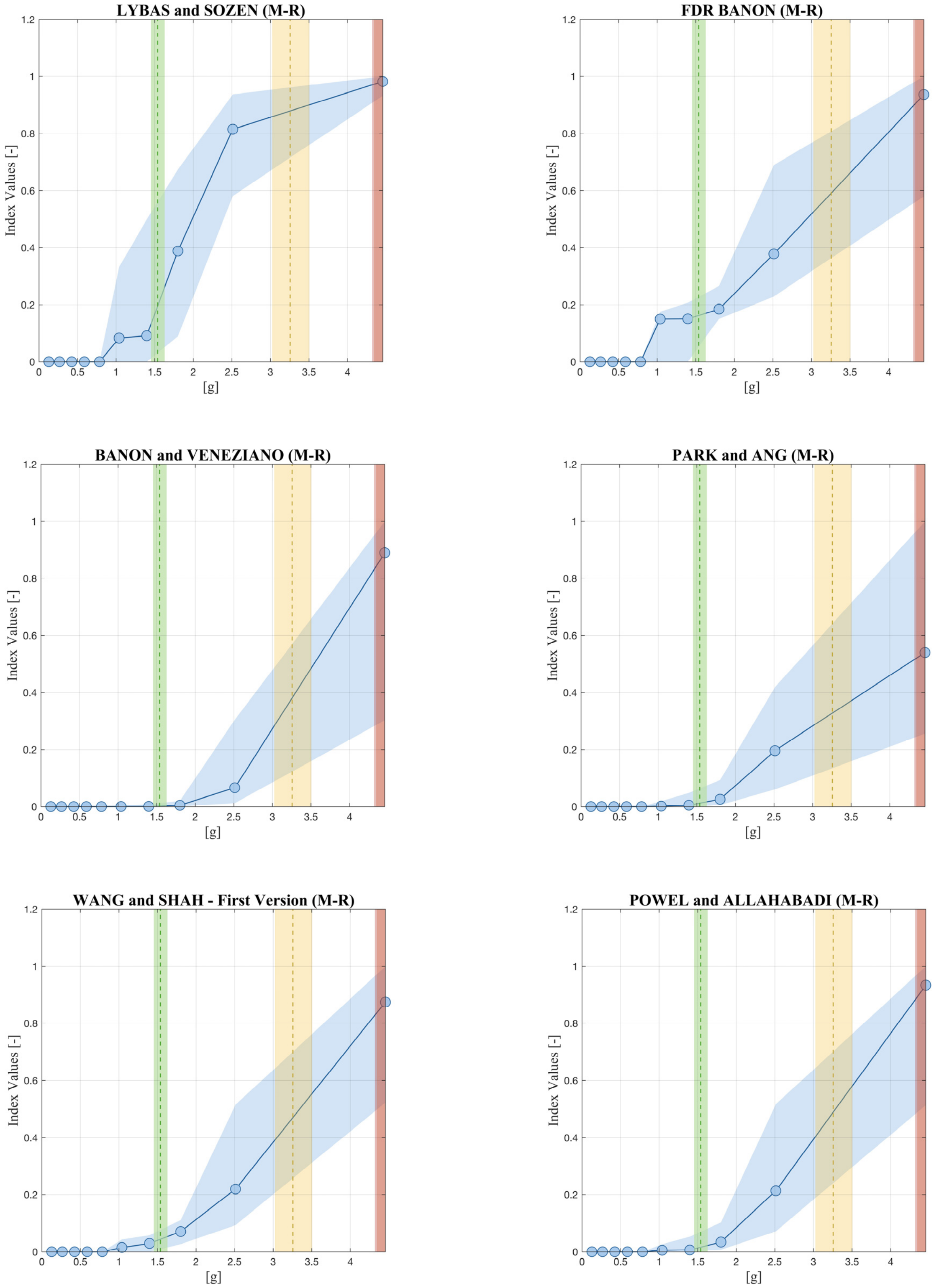

Figure A6. Damage indexes for the code-conforming SW building in the infilled frame configuration (CC_W_IF). Note: the green, yellow, orange and red refer to the UPD, LS, CP and GC performance levels, respectively.

Appendix B

Table A1. Overview of the range, dispersion (D) and overlap (O) of all damage indexes for each limit state for the EX_MRF_BF building based on MR values.

	UPD				LS				CP				GC		
Index	**Min**	**Max**	**D [%]**	**O_1 [%]**	**Min**	**Max**	**D [%]**	**O_2 [%]**	**Min**	**Max**	**D [%]**	**O_3 [%]**	**Min**	**Max**	**D [%]**
L-S	0.00	0.05	4.2	0.0	0.79	0.88	9.0	0.0	0.92	0.99	6.9	96.9	0.92	0.99	7.0
FDR	0.02	0.22	20.6	0.0	0.88	0.92	4.4	18.1	0.91	0.99	7.3	94.7	0.92	0.99	7.3
B-V	0.00	0.01	0.9	0.0	0.54	0.69	14.4	0.0	0.87	0.98	11.3	79.8	0.89	0.99	9.6
P-A	0.00	0.00	0.0	0.0	0.12	0.37	25.1	0.0	0.43	0.86	43.0	94.4	0.45	0.90	44.8
W-S-1	0.00	0.02	1.9	0.0	0.62	0.73	11.0	0.0	0.77	0.98	20.4	80.5	0.81	0.98	17.1
P-Al	0.00	0.02	1.7	0.0	0.62	0.76	13.3	0.0	0.90	0.99	8.7	80.1	0.92	0.99	7.4

Table A2. Overview of the range, dispersion (D) and overlap (O) of all damage indexes for each limit state for the EX_MRF_IF building based on MR values.

	UPD				LS				CP				GC		
Index	**Min**	**Max**	**D [%]**	**O_1 [%]**	**Min**	**Max**	**D [%]**	**O_2 [%]**	**Min**	**Max**	**D [%]**	**O_3 [%]**	**Min**	**Max**	**D [%]**
L-S	0.00	0.28	27.6	0.0	0.29	1.00	71.0	11.8	0.92	1.00	8.4	64.7	0.95	1.00	5.4
FDR	0.00	0.06	6.4	0.0	0.25	1.00	75.3	25.6	0.81	1.00	19.3	64.7	0.88	1.00	12.5
B-V	0.00	0.12	12.3	0.0	0.32	1.00	68.4	2.9	0.98	1.00	2.0	64.7	0.99	1.00	1.3
P-A	0.00	0.13	13.2	0.0	0.27	1.00	73.3	19.2	0.86	1.00	14.1	64.7	0.91	1.00	9.1
W-S-1	0.00	0.04	3.9	0.0	0.31	1.56	125	38.5	1.08	1.56	48.0	64.7	1.25	1.56	31.0
P-Al	0.00	0.06	6.4	0.0	0.25	1.00	75.3	25.6	0.81	1.00	19.3	64.7	0.88	1.00	12.5

Table A3. Overview of the range, dispersion (D) and overlap (O) of all damage indexes for each limit state for the CC_MRF_BF building based on MR values.

	UPD				LS				CP				GC		
Index	**Min**	**Max**	**D [%]**	**O_1 [%]**	**Min**	**Max**	**D [%]**	**O_2 [%]**	**Min**	**Max**	**D [%]**	**O_3 [%]**	**Min**	**Max**	**D [%]**
L-S	0.00	0.00	0.0	0.0	0.45	0.68	23.4	0.0	0.86	0.99	12.5	91.4	0.87	1.00	12.6
FDR	0.00	0.00	0.0	0.0	0.35	0.49	14.0	0.0	0.73	0.97	23.4	86.1	0.77	1.00	23.4
B-V	0.00	0.00	0.0	0.0	0.05	0.12	7.2	0.0	0.54	0.94	40.7	66.7	0.67	1.00	32.8
P-A	0.00	0.00	0.0	0.0	0.01	0.05	4.7	0.0	0.14	0.80	66.2	93.6	0.18	1.00	81.9
W-S-1	0.00	0.00	0.0	0.0	0.39	0.46	7.4	0.0	0.72	0.96	23.9	70.4	0.79	1.00	20.7
P-Al	0.00	0.00	0.0	0.0	0.13	0.25	11.7	0.0	0.66	0.96	30.3	65.5	0.76	1.00	23.8

Table A4. Overview of the range, dispersion (D) and overlap (O) of all damage indexes for each limit state for the CC_MRF_IF building based on MR values.

	UPD				LS				CP				GC		
Index	**Min**	**Max**	**D [%]**	**O_1 [%]**	**Min**	**Max**	**D [%]**	**O_2 [%]**	**Min**	**Max**	**D [%]**	**O_3 [%]**	**Min**	**Max**	**D [%]**
L-S	0.00	0.23	23.4	0.0	0.41	0.83	41.8	48.3	0.63	1.00	37.0	100	0.55	1.00	44.9
FDR	0.00	0.19	19.2	0.0	0.28	0.61	32.9	53.1	0.43	1.00	56.9	100	0.37	1.00	62.7
B-V	0.00	0.01	1.5	0.0	0.03	0.26	23.7	73.5	0.09	1.00	91.2	100	0.06	1.00	94.4
P-A	0.00	0.01	1.4	0.0	0.03	0.21	18.1	78.3	0.07	1.00	93.2	100	0.05	1.00	95.1
W-S-1	0.00	0.21	21.0	0.0	0.23	0.51	27.3	53.4	0.36	1.00	63.9	100	0.31	1.00	68.6
P-Al	0.00	0.05	4.8	0.0	0.08	0.42	33.2	61.0	0.21	1.00	78.7	100	0.15	1.00	85.0

Table A5. Overview of the range, dispersion (D) and overlap (O) of all damage indexes for each limit state for the CC_W_BF building based on MR values.

	UPD				LS				CP				GC		
Index	**Min**	**Max**	**D [%]**	**O_1 [%]**	**Min**	**Max**	**D [%]**	**O_2 [%]**	**Min**	**Max**	**D [%]**	**O_3 [%]**	**Min**	**Max**	**D [%]**
L-S	0.00	0.10	9.9	0.0	0.81	0.94	12.8	0.5	0.94	1.00	5.7	87.1	0.95	1.00	5.1
FDR	0.00	0.07	6.6	0.0	0.44	0.81	36.1	5.8	0.78	0.99	20.7	87.1	0.81	0.99	18.3
B-V	0.00	0.00	0.2	0.0	0.09	0.49	40.4	0.0	0.56	0.99	43.0	87.6	0.61	0.99	37.9
P-A	0.00	0.00	0.3	0.0	0.12	0.36	24.1	0.0	0.42	0.91	49.0	88.7	0.47	0.93	45.8
W-S-1	0.00	0.01	1.4	0.0	0.26	0.65	39.3	0.0	0.70	0.98	28.2	87.7	0.74	0.99	25.2
P-Al	0.00	0.01	1.0	0.0	0.25	0.65	40.1	0.0	0.71	0.99	28.4	87.6	0.74	0.99	25.1

Table A6. Overview of the range, dispersion (D) and overlap (O) of all damage indexes for each limit state for the CC_W_IF building based on MR values.

	UPD				LS				CP				GC		
Index	**Min**	**Max**	**D [%]**	**O_1 [%]**	**Min**	**Max**	**D [%]**	**O_2 [%]**	**Min**	**Max**	**D [%]**	**O_3 [%]**	**Min**	**Max**	**D [%]**
L-S	0.01	0.60	58.6	0.0	0.67	0.97	29.5	19.2	0.91	1.00	8.8	100	0.91	1.00	9.2
FDR	0.02	0.24	21.9	0.0	0.32	0.85	52.5	54.7	0.56	1.00	44.0	100	0.56	1.00	44.5
B-V	0.00	0.01	1.5	0.0	0.09	0.66	56.9	65.4	0.29	1.00	71.4	100	0.28	1.00	71.8
P-A	0.00	0.07	7.3	0.0	0.11	0.71	60.2	78.0	0.24	1.00	75.5	100	0.24	1.00	75.8
W-S-1	0.00	0.09	8.4	0.0	0.21	0.76	55.5	47.4	0.50	1.00	50.1	100	0.49	1.00	50.7
P-Al	0.00	0.08	8.0	0.0	0.19	0.76	57.4	47.7	0.49	1.00	51.1	100	0.48	1.00	51.7

References

1. Angiolilli, M.; Eteme Minkada, M.; Di Domenico, M.; Cattari, S.; Belleri, A.; Verderame, G.M. Comparing the Observed and Numerically Simulated Seismic Damage: A Unified Procedure for Unreinforced Masonry and Reinforced Concrete Buildings. *J. Earthq. Eng.* **2022**, *28*, 1157–1193. [CrossRef]
2. Williams, M.S.; Sexsmith, R.G. Seismic damage indeces for concrete structures: A state-of-the-art review. *Earthq. Spectra* **1995**, *11*, 319–349. [CrossRef]
3. Chung, Y.S.; Meyer, C.; Shinozuka, M. *Seismic Damage Assessment of Reinforced Concrete Members*; Technical Report NCEER 97-0022; State University of New York at Buffalo: Buffalo, NY, USA, 1987.
4. Lybas, J.; Sozen, M. *Effect of Beam Strength and Stiffness on the Dynamic Behavior of Reinforced Concrete Coupled Walls*; Civil Engineering Studies, Structural Research Series No. 444; University of Urbana: Champaign, IL, USA, 1977.
5. Banon, H.; Irvine, H.M.; Biggs, J.M. Seismic damage in reinforced concrete frames. *J. Struct. Div.* **1981**, *107*, 1713–1729. [CrossRef]
6. Banon, H.; Veneziano, D. Seismic safety of reinforced concrete members and structures. *Earthq. Eng. Struct. Dyn.* **1982**, *10*, 179–193. [CrossRef]
7. Hwang, T.H.; Scribner, C.F. R/C member cyclic response during various loadings. *J. Struct. Eng.* **1984**, *110*, 477–489. [CrossRef]
8. Park, Y.J.; Ang, A.H.-S. Mechanistic seismic damage model for reinforced concrete. *J. Struct. Eng.* **1985**, *111*, 722–739. [CrossRef]
9. Stephens, J.E.; Yao, J.T.P. Damage assessment using response measurements. *J. Struct. Eng.* **1987**, *113*, 787–801. [CrossRef]
10. Wang, M.-L.; Shah, S.P. Reinforced concrete hysteresis model based on the damage concept. *Earthq. Eng. Struct. Dyn.* **1987**, *15*, 993–1003. [CrossRef]
11. Powell, G.H.; Allahabadi, R. Seismic damage prediction by deterministic methods: Concept and procedures. *Earthq. Eng. Struct. Dyn.* **1998**, *16*, 719–734. [CrossRef]
12. DiPasquale, E.; Cakmak, A.S. *Identification of the Serviceability Limit State and Detection of Seismic Structural Damage*; Technical Report NCEER-88-0022; State University of New York, Buffalo: Buffalo, NY, USA, 1989.
13. Bracci, J.M.; Reinhorn, A.M.; Mander, J.B.; Kunnath, S.K. *Deterministic Model for Seismic Damage Evaluation of Reinforced Concrete Structures*; Technical Report NCEER-89-0033; State University of New York, Buffalo: Buffalo, NY, USA, 1989.
14. Colombo, A.; Negro, P. A damage index of generalised applicability. *Eng. Struct.* **2005**, *27*, 1164–1174. [CrossRef]
15. Rodriguez, M.E.; Padilla, D. A damage index for the seismic analysis of reinforced concrete members. *J. Earthq. Eng.* **2009**, *13*, 364–383. [CrossRef]
16. Ladinović, D.; Radujković, A.; Raŝeta, A. Seismic performance assessment based on damage of structures-part 1: Theory. *Archit. Civ. Eng.* **2011**, *9*, 77–88.

17. Mahin, S.A.; Bertero, V.V. An evaluation of inelastic seismic design spectra. *J. Struct. Eng.* **1981**, *107*, 1775–1795. [CrossRef]
18. Guo, J.; Wang, J.J.; Li, Y.; Zha, W.G.; Du, Y.L. Three-dimensional extension for Park and Ang damage model. *Structures* **2016**, *7*, 184–194. [CrossRef]
19. Midas GEN. Analysis Manual for Midas GEN. 2022. Available online: https://manual.midasuser.com/KR/Gen/935/whnjs.htm (accessed on 9 April 2024).
20. McKenna, F.; Fenves, G.L. OpenSees Manual. 2013. Available online: https://opensees.berkeley.edu/wiki/index.php/Command_Manual (accessed on 8 May 2024).
21. Ibarra, L.F.; Medina, R.A.; Krawinkler, H. Hysteretic models that incorporate strength and stiffness deterioration. *Earthq. Eng. Struct. Dyn.* **2005**, *34*, 1489–1511. [CrossRef]
22. Decanini, L.D.; Gavarini, C.; Bertoldi, S.H. Telai tamponati soggetti ad azioni sismiche, un modello semplificato: Confronto sperimentale e numerico. In Proceedings of the VI Italian National Seismic Engineering Conference, Perugia, Italy, 13–15 October 1993.
23. da Porto, F.; Donà, M.; Verlato, N.; Guidi, G. Experimental Testing and Numerical Modelling of Robust Unreinforced and Reinforced Clay Masonry Infill Walls, With and Without Openings. *Front. Built Environ.* **2020**, *6*, 591985. [CrossRef]
24. Sassun, K.; Sullivan, T.J.; Morandi, P.; Cardone, D. Characterising the in-plane seismic performance of infill masonry. *Bull. N. Z. Soc. Earthq. Eng.* **2016**, *49*, 100–117. [CrossRef]
25. Hak, S.; Morandi, P.; Magenes, G. *Damage Control of Masonry Infills in Seismic Design*; Research EUCENTRE, 2013/1; IUSS Press: Pavia, Italy, 2013.
26. Cornell, C.A.; Jalayer, F.; Hamburger, R.O.; Foutch, D.A. Probabilistic basis for 2000 SAC federal emergency management agency steel moment frame guidelines. *J. Struct. Eng.* **2002**, *128*, 526–533. [CrossRef]
27. *EN 1998-1:2004*; Eurocode 8: Design of Structures for Earthquake Resistance—Part 1: General Rules, Seismic Actions and Rules for Buildings. European Committee for Standardization: Brussels, Belgium, 2004.
28. Iervolino, I. *The Implicit Seismic Risk of Code-Conforming Structures in Italy—A Joint ReLUIS-EUCENTRE Project*; Results of the 2015–2017; RINTC Workgroup: Naples, Italy, 2018.
29. Iervolino, I.; Baraschino, R.; Belleri, A.; Cardone, D.; Della Corte, G.; Franchin, P.; Lagomarsino, S.; Magliulo, G.; Andrea Marchi Penna, A.; Viggiani, L.R.S.; et al. Seismic Fragility of Italian Code- Conforming Buildings by Multi-Stripe Dynamic Analysis of Three-Dimensional Structural Models. *J. Earthq. Eng.* **2023**, *27*, 4415–4448. [CrossRef]
30. Baker, J.W. Conditional Mean Spectrum: Tool for ground motion selection. *J. Struct. Eng.* **2011**, *137*, 322–331. [CrossRef]